5-11-2006

Formation of an anisotropy lattice in Co/Pt multilayers by direct laser interference patterning

Aliekber Aktag
Abant Izzet Baysal University, Bolu, Turkey, aeaktag@hotmail.com

Steven A. Michalski
University of Nebraska-Lincoln, smichalski2@unl.edu

Lanping Yue
University of Nebraska-Lincoln, lyue2@unl.edu

Roger D. Kirby
University of Nebraska-Lincoln, rkirby1@unl.edu

Sy_Hwang Liou
University of Nebraska-Lincoln, sliou@unl.edu

Formation of an anisotropy lattice in Co/Pt multilayers by direct laser interference patterning

Aliekber Aktag[a)]
Department of Physics, Abant Izzet Baysal University, Bolu 14280, Turkey

Steven Michalski, Lanping Yue, Roger D. Kirby, and Sy-Hwang Liou
Department of Physics and Astronomy, University of Nebraska, Lincoln, Nebraska 68588-0111
and Center for Materials Research and Analysis, University of Nebraska, Lincoln, Nebraska 68588-0111

(Received 10 January 2006; accepted 8 March 2006; published online 11 May 2006)

We report on the use of direct laser interference patterning to form an "anisotropy" lattice in Co/Pt thin film multilayers. Co/Pt multilayers have been extensively studied and, for the compositions studied here, are characterized by strong perpendicular magnetic anisotropy in which the magnetic moment is perpendicular to the film plane. In direct laser interference patterning, two-to-four coherent laser beams from a pulsed Nd:YAG laser strike the sample surface simultaneously, and for sufficiently intense beams the sample properties are modified locally where interference maxima occur. Kerr rotation, magnetic force microscopy, and atomic force microscopy measurements after patterning by one pulse from the laser show that the films have a regular array of "dots" with in-plane magnetization in a background matrix of perpendicular magnetization. Such patterning holds promise for the study of model nanoscale magnetic systems. © *2006 American Institute of Physics*. [DOI: 10.1063/1.2191747]

I. INTRODUCTION

There has been much interest in recent years in developing two- and three-dimensional arrays of magnetic particles or features because of their interesting physics and potential applications in such areas as high-density information storage, sensors, and actuators. A number of techniques including electron-beam lithography,[1] extreme uv photolithography,[2] direct imprint patterning,[3] various self-assembly methods,[4–9] and ion-beam milling/mixing[10–16] have been used to fabricate small magnetic structures and arrays, and these techniques are leading both to a better understanding of the physics associated with arrays of small magnetic structures and to the potential for improved information storage and other technologies.[17–21] Martín *et al.* have provided a comprehensive review of many of these techniques, with an emphasis on fabrication of ordered magnetic nanostructures.[22] We report here on the use of direct laser interference patterning (DLIP) to form arrays of magnetic dots with unique properties in Co/Pt multilayers. Direct laser interference patterning was developed by Polushkin and co-workers,[23–30] and it involves using interference between several coherent laser beams to locally modify properties of thin metal films. In contrast to most nanoscale fabrication techniques, DLIP employs direct and local modification of material properties, rather than lithography, to form dot and antidot arrays and even more complex structures. As will be seen DLIP is a powerful emerging tool to form interesting and potentially useful magnetic structures.

The focus of this paper is on Co/Pt multilayers, which have been the subject of much attention because they are attractive candidates for ultrahigh-density information storage applications. The literature on the magnetic properties of Co/Pt is very extensive, and we present here a brief summary of some major observations. Li and Garcia demonstrated that Co/Pt multilayer films have a large Kerr rotation,[31] attributed to the magneto-optic response associated with induced magnetic polarization in the nonmagnetic Pt sublayers.[32] Suzuki *et al.* studied the coercivity mechanism of Co/Pt multilayers prepared under various substrate conditions. They found that wall pinning is a major factor for high coercivity and squareness in Co/Pt multilayers. With less interfacial sharpness, the size of pinning centers increases. They proposed that inhomogeneities near the interface between Co and Pt play a major role as pinning sites for wall motion.[33] Hatwar and Brucker studied the microstructure and the magnetic properties of the Co/Pt multilayers by varying the deposition condition (morphology) of the underlayer. Underlayer morphology is controlled by sputtering pressure for optimum combination of coercivity and squareness. They found that a smooth underlayer deposited at low pressure results in high squareness but low coercivity, whereas a rough underlayer deposited at high pressure produces Co/Pt films with low squareness but high coercivity.[34] Shen *et al.* studied the magnetization reversal through magnetization time dependence and direct domain observations of Co/Pt multilayers with different numbers of bilayers. They found that magnetization reversal occurs through rare nucleation events following fast domain expansion. The expansion process is likely controlled by presence of defects and the defects may originate from the roughness of the interface between Co and Pt.[35]

In experiments somewhat akin to the experiments presented here, Bernas and co-workers used ion-beam mixing to locally alter the coercivity of Pt/Co/Pt trilayers with perpendicular magnetic anisotropy.[36–38] Evidently, interface mixing

[a)]Electronic mail: aeaktag@hotmail.com

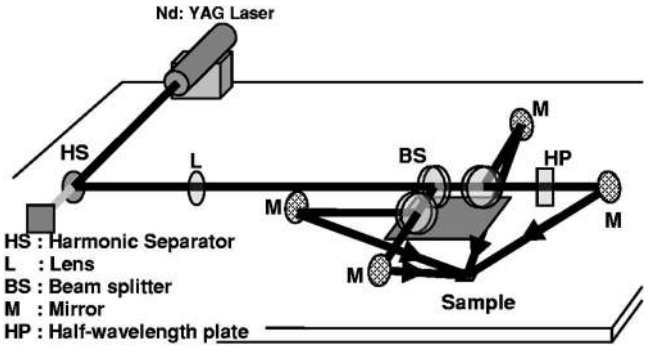

FIG. 1. Direct laser interference patterning apparatus. 100 mJ, 5 ns pulses from a Nd:YAG laser are split into two-to-four equal-intensity beams which interfere at the samples. The harmonic separator (HS) selects 532 nm wavelength, the lens L permits adjustment of the light intensity at the sample surface, three 50% beam splitters (BS) create the four beams, which are directed to the sample surface by mirrors (M), and half-wave plates (HP) can be inserted to convert *p*-polarized light to *s*-polarized light.

caused by He^+ irradiation reduces the magnetic anisotropy substantially, leading to reduced coercivity. Terris *et al.* irradiated Co/Pt multilayers (perpendicular magnetic anisotropy) with He^+, Ar^+, and N^+ through a silicon stencil mask and found that they could form ~ 1 μm dots which had in-plane magnetization.[39,40] As will be seen, our experiments achieve similar results using purely optical patterning techniques.

II. DIRECT LASER INTERFERENCE PATTERNING

A schematic diagram of the optical system used to pattern magnetic thin films is shown in Fig. 1. A continuum Surelite Nd:YAG (yttrium aluminum garnet) laser provides 5 ns pulses of wavelength 1064 or 532 nm with pulse energies in the range of 100–400 mJ. For the work on Co/Pt presented here, 532 nm light was used exclusively. The beam from the laser passes through a lens, which is used to vary the light intensity reaching the sample surface, and then through a series of 50% beam splitters. This optical configuration results in four approximately equal-intensity beams striking the sample. The angles of incidence can be varied independently, as can the polarizations of the beams through the use of half-wave plates. When the beams arrive at the sample surface, optical interference occurs, and local heating at the interference maxima can modify the local material properties or even partially ablate the sample if a high light intensity is used. For the results presented here on Co/Pt multilayers, modest light intensities were used and no ablation was observed. Regions typically 3–4 mm in lateral dimensions could be patterned with one pulse of the laser.

A. Two-beam interference

Two beams approach the sample surface from opposing directions with identical angles of incidence θ. As is easily seen in Fig. 2(a), the light intensity at the surface varies sinusoidally with position, with fringe spacing being $\lambda/[2\sin(\theta)]$. For *s*-polarized light, the fringe contrast is ideally 100%, while for *p*-polarized light the contrast is less than 100%, depending on the angles of incidence. Figure 2(b) shows an optical microscopy image of lines formed by

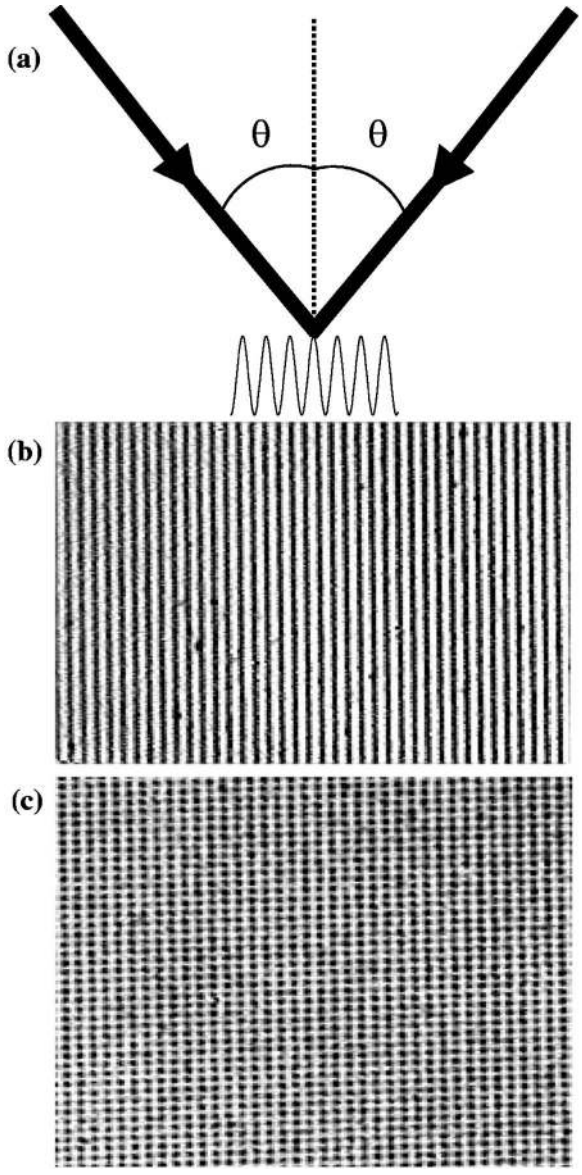

FIG. 2. Two-beam interference. (a) Light intensity as a function of position, (b) optical microscopy image of a Co–C film after partial ablation by one pulse of the laser, and (c) optical microscopy image of a Co–C film which was subjected to one pulse from the laser, then rotated through a 90° angle, and subjected to a second pulse.

partial ablation of a Co–C film by one pulse from the laser. Two-dimensional arrays can be formed by first irradiating the sample with one pulse from the laser, then rotating the sample through an angle of 90°, and then irradiating with a second pulse, as shown in Fig. 2(c) for a Co–C film.

By using more than two beams and differing angles of incidence and beam polarizations, a variety of two-dimensional arrays can be formed. We have developed a program using the algebraic computer program MAPLE to simulate the interference effects which occur when more than two beams interfere on the sample surface. This program simply sums the electric field vectors of the two-to-four beams at their intersection to calculate the spatial dependence of the light intensity at the surface. In what follows, we give a few examples of these simulations.

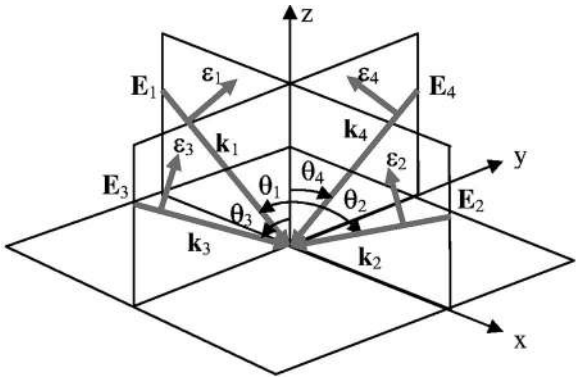

FIG. 3. Direct laser interference patterning geometry. Plane waves 1 and 2 propagate in the xz plane at angles of incidence θ_1 and θ_2, while plane waves 3 and 4 propagate in the yz plane with angles of incidence θ_3 and θ_4.

B. Four-beam interference

Figure 3 shows the geometry used to carry out the simulations. Plane waves 1 and 2 propagate in the (xz) plane at angles of incidence θ_1 and θ_2, while plane waves 3 and 4 propagate in the (yz) plane with angles of incidence θ_3 and θ_4. The vector sums of the electric field vectors are calculated in the (xy) plane. In all simulations presented in this subsection, the four beams are assumed to have 532 nm wavelength and the same electric field amplitudes.

Figures 4(a)–4(h) show simulated interference patterns when four beams interfere, with white indicating high light intensity. In Figs. 4(a) and 4(c), all angles of incidence are 35°, while in Figs. 4(b) and 4(d) all angles of incidence are 60°. In Figs. 4(a) and 4(b), the beams all have p polarization, and in Figs. 4(c) and 4(d), they all have s polarization. It is interesting to note that Fig. 4(b) shows "dots," while Fig. 4(a) shows "antidots."

Figures 4(e)–4(g) show patterns obtained when the angles of incidence are 30° for x-directed beams and 60° for the y-directed beams. In Fig. 4(e), all beams have p polarization and in Fig. 4(f), they all have s polarization. In Fig. 4(g), the x-directed beams have p polarization, while the y-directed beams have s polarization. Finally, Fig. 4(h) corresponds to when the beams all have p polarization, while the angles of incidence are 60° for the x-directed beams and 50° and 15° for the two y-directed beams.

The examples above show that the symmetries of the interference maxima depend both on the angles of incidence and the beam polarizations and that a wide variety of patterns can be obtained. A noticeable problem arises when one or two of the four beams are misaligned slightly (out of the plane of incidence). This is shown schematically in Fig. 5(a), where a secondary periodicity is observed in optical microscopy for a partially ablated codeposited Co–C film. Figure 5(b) shows a simulated pattern when beams are misaligned by 3°. There is good qualitative agreement, suggesting that such misalignment is the origin of the secondary periodicity.

C. Three-beam interference

Because of the difficulty in aligning four beams sufficiently well to avoid secondary periodicities, we most often used a three-beam interference configuration, where one of the four beams (beam 1 in Fig. 3) is simply removed. Simulated patterns for all angles of incidence equal to 60° for all p polarizations are shown in Fig. 6(a) and x-directed s polarization and y-directed p polarizations in Fig. 6(b), while simulated patterns when the angles of incidence of all p-polarizations x-directed beam at 30° angle of incidence and y-directed beams at 60° angles of incidence are shown in Fig. 6(c), and x-directed s-polarization beam at 60° angles of incidence and y-directed p-polarization beams at 30° angles of incidence are in Fig. 6(d). Note that dots are converted to antidots simply by changing the polarization of the y-directed beam from p to s.

III. EXPERIMENT AND RESULTS

A. Structural and magnetic properties of Co/Pt multilayers

We used magnetron sputtering to deposit Co/Pt multilayer films on a smooth (100) Si wafer at low Ar pressure (5 mTorr) for several different bilayers and film thicknesses. All films were protected by a 20 nm thick SiO_x overcoat. The hysteresis loops of films showed a good degree of squareness, but low coercivities. Among these, the [Co(4 Å)/Pt(10 Å)] films with 7–11 bilayers had a coercivity in the 100–200 Oe range and seemed ideally suited for this study. The penetration depth of the laser light is similar to the total film thickness, so that local changes caused by local interference maxima should extend through the thickness of the film.

One pulse from the Nd:YAG laser (532 nm) was used to pattern a roughly 3 mm diameter area of a $[\mathrm{Co}(4\ \text{Å})/\mathrm{Pt}(10\ \text{Å})]\times 11$ film. The pattern was obtained by interference of three linearly polarized beams at 25° angles of incidence. The two x-directed beams were p polarization, while the y directed beam was s polarization. The laser pulse energy was small enough that no topographical changes were observed in atomic force microscopy (AFM) measurements, that is, no ablation occurred.

Figures 7(a) and 7(b) show low-angle x-ray diffraction scans from the as-deposited and patterned regions of the $[\mathrm{Co}(4\ \text{Å})/\mathrm{Pt}(10\ \text{Å})]\times 11$ film, respectively. The as-deposited film shows a well-defined peak due to the 14 Å bilayer thickness at $2\theta=6.9°$, and multiple reflection peaks due to the total Co/Pt thickness at lower angles. The scan from the patterned region also shows the bilayer peak, but at smaller intensity and with an increase in width. These results suggest less abrupt interfaces between Co and Pt layers after patterning. The multiple reflection peaks from the patterned film have less contrast, suggesting either that there is increased surface roughness or that the dots and matrix have subtly different effects on the x rays. It should be noted that no topographical changes due to patterning are observed in AFM measurements (Sec. III B), but the SiO_x overcoat reduces our sensitivity to small changes.

We attempted high-resolution transmission electron microscopy measurements to investigate changes which occur upon patterning. These measurements were not very infor-

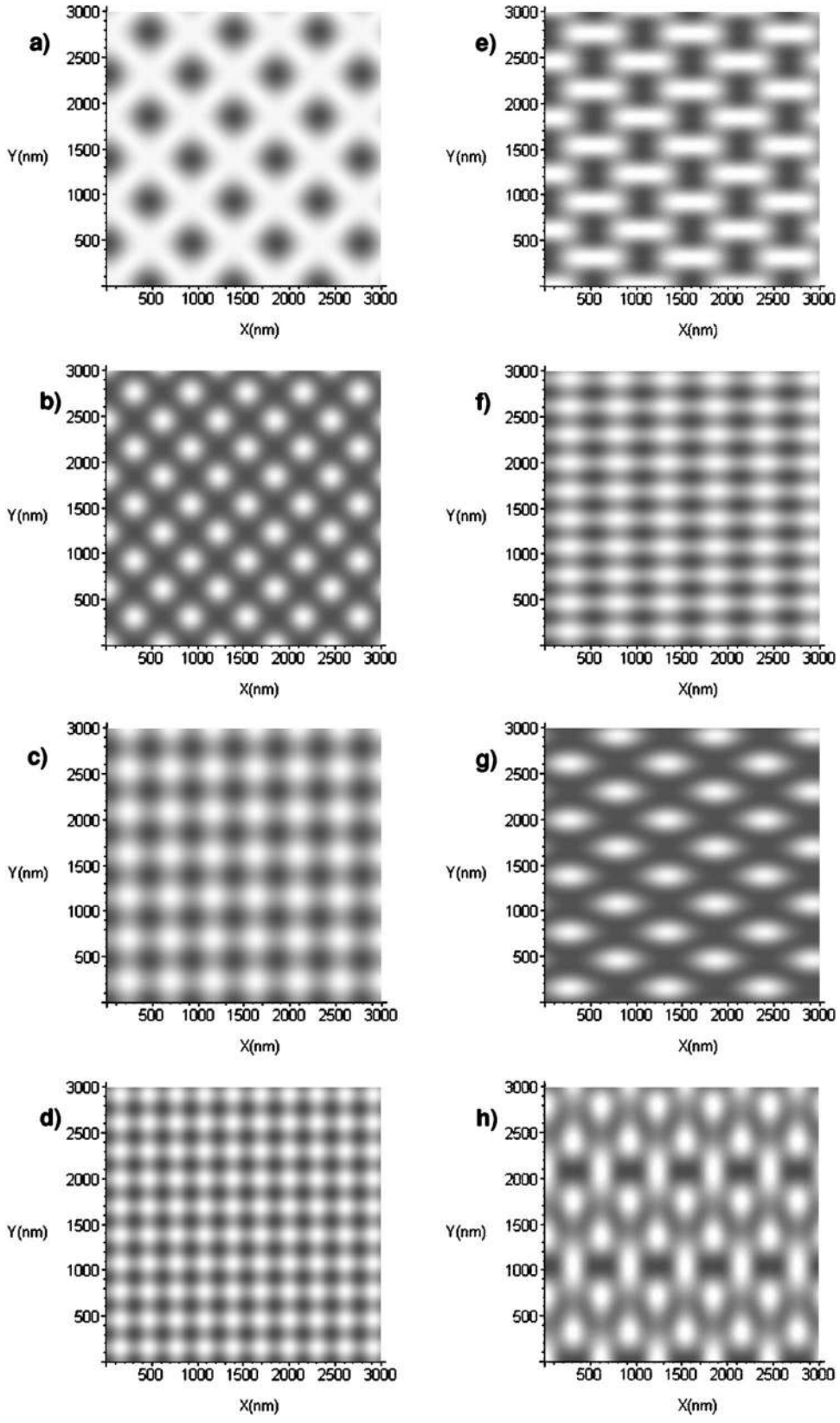

FIG. 4. Simulated four-beam interference patterns when all beams have *p* polarization and all angles of incidence are (a) 35° and (b) 60°. All beams have *s* polarization and all angles of incidence are (c) 35° and (d) 60°. Simulated four-beam interference patterns. Interference patterns when the angles of incidence for *x*-directed beams are 30°, while for the *y*-directed beams are 60°, (e) all beams have *p* polarization, (f) all beams have *s* polarization, and (g) the two *x*-directed beams have *p* polarization and the two *y*-directed beams have *s* polarization. For (h) all beams have *p* polarization and the angles of incidence for *x*-directed beams are 60°, while for the *y*-directed beams they are 50° and 15°.

mative, as no differences could be observed between the dot regions and the background/matrix regions. Any structural changes must be quite subtle.

Figures 8(a) and 8(b) show polar Kerr rotation measurements at room temperature for as-deposited and patterned regions of the film, respectively. The polar Kerr measurements on the as-deposited film show the typical square hysteresis loop for Co/Pt multilayers of this composition, with essentially 100% squareness and a coercivity of 105 Oe. This loop is similar to loops reported by others for Co/Pt multilayers of similar bilayer thickness. Figure 8(b) shows the polar Kerr effect in the patterned region of the film. Note that the range of magnetic field is between ±8 kOe, or much larger than in Fig. 8(a). The loop in Fig. 8(b) shows a re-

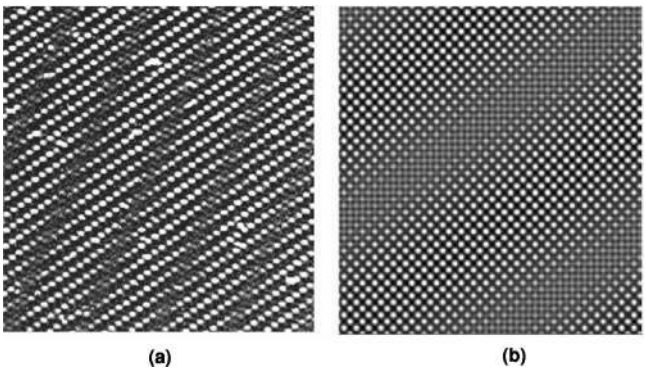

FIG. 5. (a) Optical microscopy image of partially ablated Co–C film showing secondary modulation pattern for an estimated 5° misalignment of beams. (b) Simulated image for 3° misalignment of beams.

duced perpendicular remanence and squareness and a very slow approach to saturation, and it is consistent with a partial conversion of the film to in-plane magnetic anisotropy.

Figures 8(c) and 8(d) show the longitudinal Kerr rotation hysteresis loops of as-deposited and patterned regions of the film, respectively. The loop for the as-deposited region is as expected for a film with perpendicular magnetic anisotropy. After patterning, the loop clearly shows a strong in-plane character, but with a slow approach to saturation indicative of a significant perpendicular magnetization component.

In review, Kerr rotation measurements indicate that the patterning process converts perpendicular magnetization into in-plane magnetization in the locally annealed regions, thereby creating an anisotropy lattice of in-plane dots in a background of perpendicular anisotropy. Additional evidence for this behavior is found in our magnetic force microscopy observations.

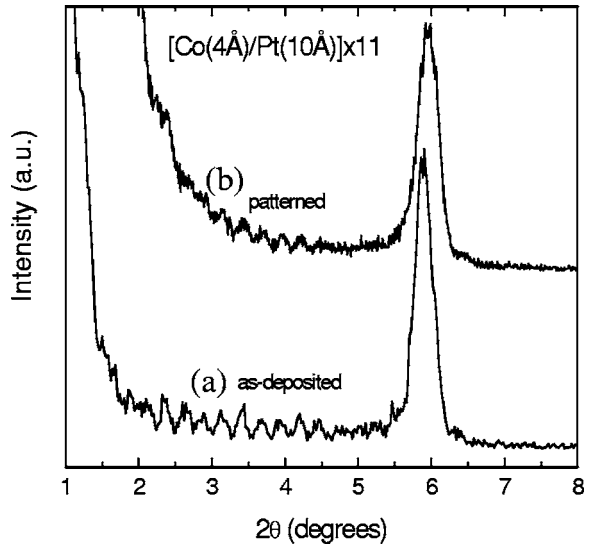

FIG. 7. Low-angle x-ray diffraction for $[Co(4\ Å)/Pt(10\ Å)]\times 11$: (a) as-deposited and (b) patterned.

B. Magnetic force microscopy

In this subsection, AFM and magnetic force microscopy (MFM) results on $Co/Pt:SiO_x$ multilayer films are presented and discussed. A Digital Instruments Dimension D3000 atomic force microscope was used to obtain all of the topographic and magnetic images presented here. The atomic force images were obtained using the tapping mode. All of the MFM images were obtained using homemade high-resolution MFM tips with high coercivity but low stray magnetic field. The tips were fabricated by deposition of about 10 nm thick CoPt film on commercially available batch-

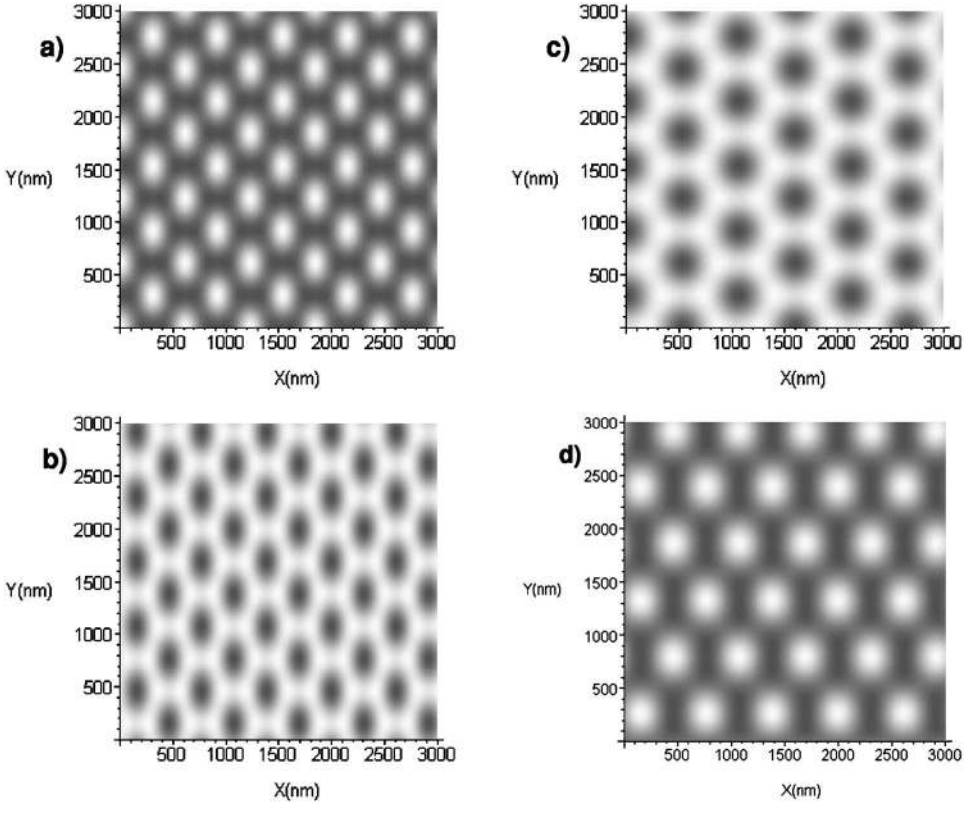

FIG. 6. Simulated three-beam interference patterns for all three beams at 60° angle of incidence. (a) All *p* polarizations, (b) *x*-directed beams are *s* polarization and *y*-directed beams are *p* polarization, (c) all beams are *p* polarization with the *x*-directed beams at 30° angle of incidence and *y*-directed beams at 60° angles of incidence, and (d) *x*-directed beam at 60° angle of incidence with *s* polarization, and *y*-directed beams at 30° angles of incidence and *p* polarization.

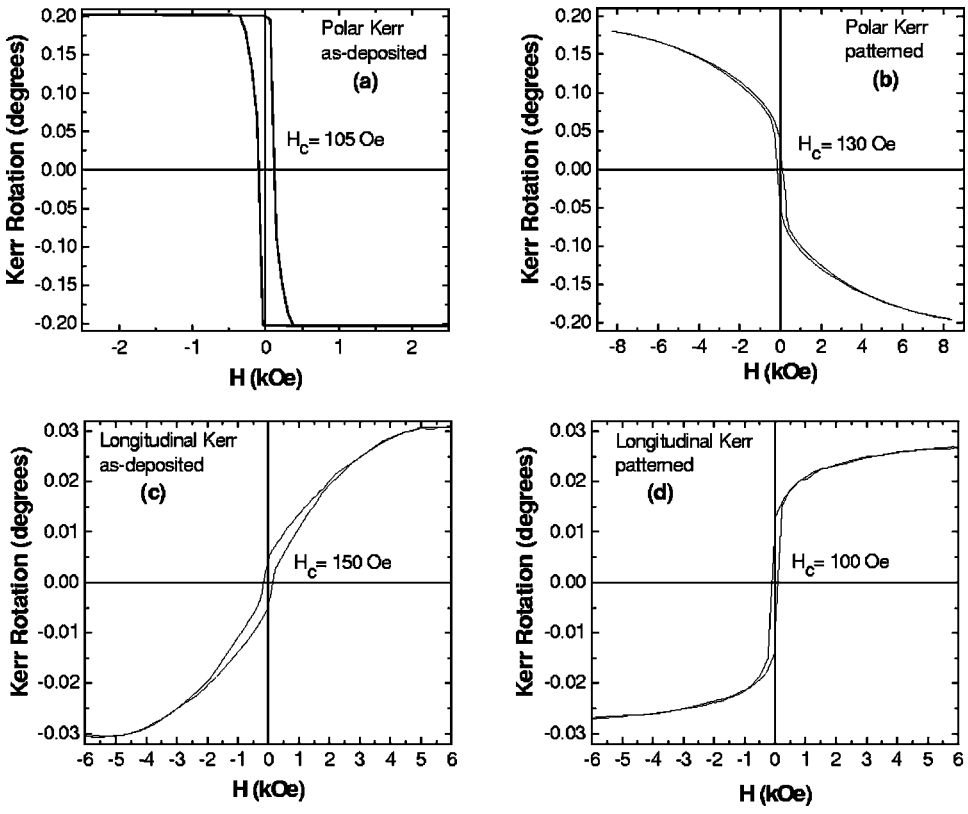

FIG. 8. (a) polar Kerr hysteresis loop for as-deposited film, (b) polar Kerr hysteresis loop for patterned film, (c) longitudinal Kerr hysteresis loop for as-deposited film, and (d) longitudinal Kerr hysteresis loop for patterned film.

fabricated micromachined cantilevers. The CoPt film has the face-centered-tetragonal structure, with coercivity in excess of 15 kOe, and thus the magnetization of the tip will not be affected by the very small stray magnetic field of the sample. These tips were also modified by focused-ion-beam milling to improve the resolution of the domain images. The magnetization of the tip was oriented to point down, or perpendicular to the sample surface. It is emphasized that the MFM tip had a coercivity of 15 kOe, so that stray fields from the sample could have no effect on the magnetization of the tip. All MFM images were taken using Digital Instruments Lift-Mode™ procedure in which the tip makes two passes across the sample. On the first pass, topographical AFM data are gathered as the tip gently taps across the surface. On the second pass, this topographical information is used to move the tip at constant height above the film surface to gather the magnetic information.

A $[\mathrm{Co}(4\ \text{Å})/\mathrm{Pt}(10\ \text{Å})]\times 7$ film (with 20 nm SiO_x overcoat) was prepared using the techniques described earlier. It was patterned using three beams, with x-direction and y-direction angles of incidence at 25°. Figure 9 shows MFM (left side) and AFM (right side) images on the patterned region of this film. Note, in particular, that dots are easily observed in the MFM scan, but that the AFM scan shows no evidence of periodic topographic changes. Thus, these images confirm that DLIP locally changes the intrinsic magnetic properties, with virtually no changes in topography. Since no topographic changes due to patterning were observed in any of our scanning probe studies of $\mathrm{Co/Pt:SiO}_x$ films, we do not show the AFM scans in subsequent images.

Figure 10 shows a series of MFM images in the presence of an applied external field out of the plane of the sample. The film had been previously saturated with a negative field of 9 kOe applied into the sample plane. The *in situ* field was applied using a homebuilt set of rotating pole permanent magnets which provide an adjustable field perpendicular to the sample plane. The maximum *in situ* field available was about 1.6 kOe, which is sufficient to switch magnetization directions in the film, but not in the MFM tip. The image in the upper left corner was taken in the remanent state, and the other images were taken in fields ranging from 183 to 1576 Oe, as labeled. The remanent state shows a complex domain structure. As the applied field is increased, dots appear with increasing clarity.

We know that the *unpatterned* film when saturated initially remains almost completely saturated in the remanent state [see Fig. 8(a)], but as seen in Fig. 10, this is not the case after patterning. The image in the remanent state shows very complicated domain structures with a trace of pattern buried in it. These results demonstrate that the patterning caused some magnetic property change. In the presence of an in-

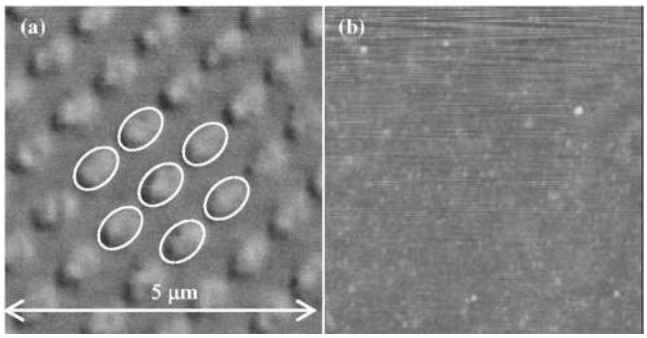

FIG. 9. (a) MFM and (b) AFM images of $[\mathrm{Co}(4\ \text{Å})/\mathrm{Pt}(10\ \text{Å})]\times 7$ film. The film has a 20 nm SiO_x overcoat. For this interference geometry, the dots are approximately ellipses of major axis of 790 nm and minor axis of 490 nm.

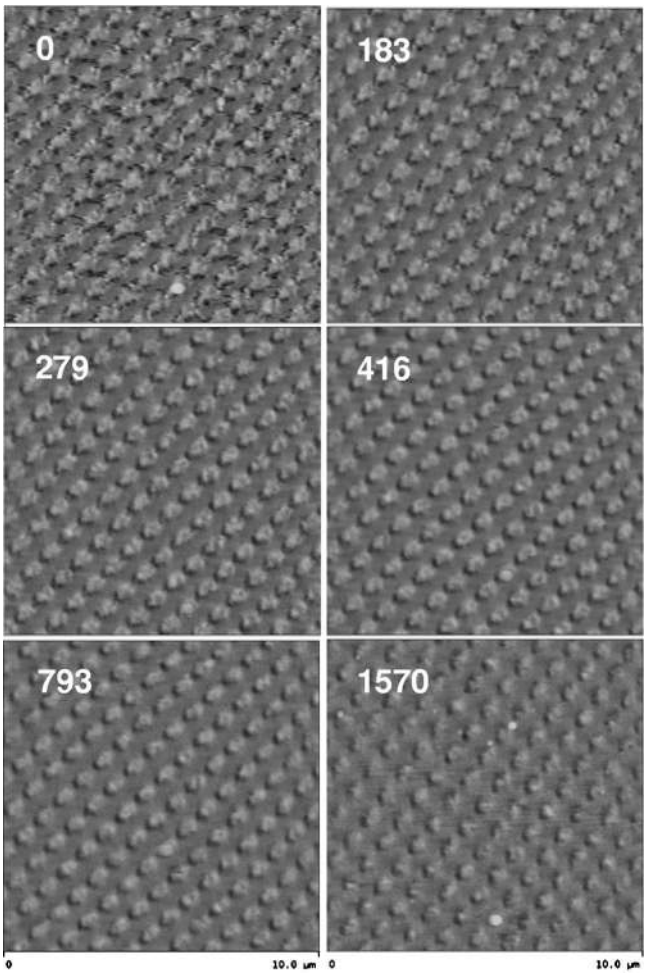

FIG. 10. MFM images of $[\mathrm{Co}(4\ \text{Å})/\mathrm{Pt}(10\ \text{Å})]\times 7$ film in various applied reversing fields, as labeled (in Oe). The image in the upper left corner was taken in remanent state after saturation in a perpendicular 9 kOe field. Each image is $10\times 10\ \mu\mathrm{m}^2$.

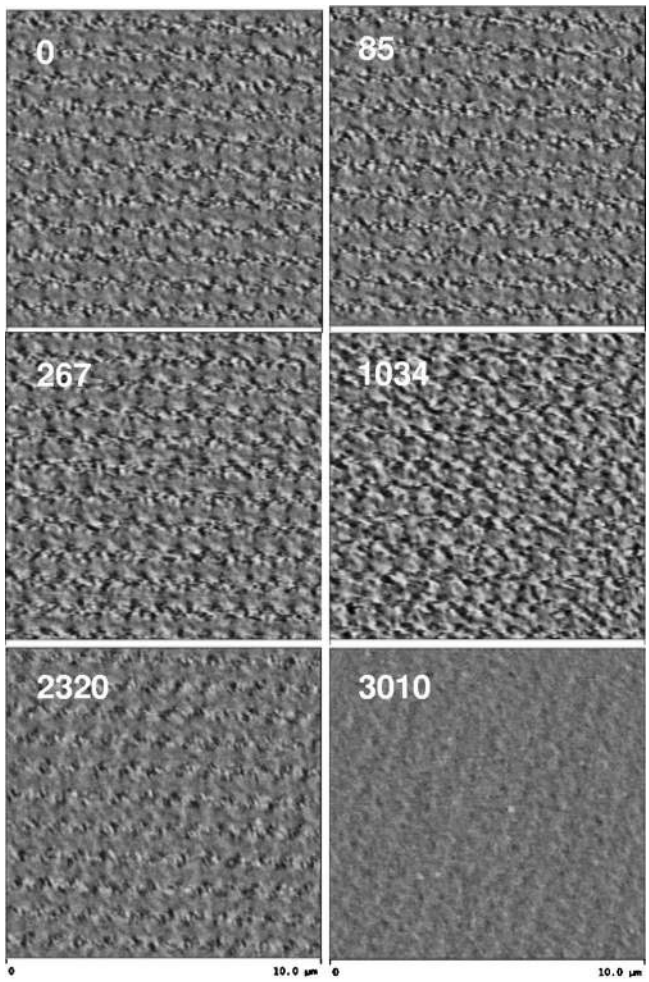

FIG. 11. MFM images of $[\mathrm{Co}(4\ \text{Å})/\mathrm{Pt}(10\ \text{Å})]\times 7$ film in various applied reversing fields, as labeled (in Oe). The image in the upper left corner was taken in the remanent state after saturation in an in-plane 3.6 kOe field. Each image is $10\times 10\ \mu\mathrm{m}^2$.

creasingly large positive applied field, the MFM images shown in Fig. 10 clearly show a pattern expected by the simulation. The dots pattern and the shortest spacing between dots, center to center (883 nm), are in good agreement with the simulation (890 nm). We note that the dots in MFM images are elliptically shaped (approximately $730\times 490\ \mathrm{nm}^2$) and have a "dark" region (attractive force) at one end and a "light" region (repulsive force) at the other. It should be remembered that the dot pattern as observed by MFM may not exactly correspond to the simulated pattern because the MFM images are the response of the tip to the stray field of the sample and its vertical derivatives as the externally applied field is changed. The response is generally quite complex. As the applied field is increased, a recognizable dot pattern, which was not obvious in the remanent state, starts to appear. Note also that the perpendicular component of the magnetization has switched somewhere between 0 and 183 Oe, since the coercivity is less than 183 Oe. That is, the area between dots still possesses strong perpendicular magnetic anisotropy (PMA) and behaves accordingly. Each dot has a dark (attractive) end and a light (repulsive) end. The dark and light contrasts along the right-diagonal direction appear to be stronger than along the left-diagonal direction. This is likely because the elliptically shaped dots are closer together in the right-diagonal direction than in the left-diagonal direction, resulting in increased magnetostatic interaction between dots. As we go to the highest available applied field, the magnetic contrast between the dots and the background diminishes substantially, which is consistent with the in-plane moments of the dots being almost completely pulled out of plane. Thus we conclude that within a dot, the moments behave as they have in-plane anisotropy, whereas the moments in region between the dots behave as perpendicular, and this is consistent with our earlier conclusion that patterning creates an anisotropy lattice in $[\mathrm{Co}(4\ \text{Å})/\mathrm{Pt}(10\ \text{Å})]\times 7$.

The $[\mathrm{Co}(4\ \text{Å})/\mathrm{Pt}(10\ \text{Å})]\times 7$ film was also studied by applying stepwise increasing or decreasing magnetic fields along dot lines in the *plane* of sample. The sample was placed in the MFM sample holder, which was surrounded by an adjustable permanent magnet. Figure 11 shows a series of MFM images. First, a 3.01 kOe field was applied to saturate the sample in the *negative* in-plane direction field along the dots. It was then decreased to zero, and a MFM scan was taken in the remanent state (upper left corner). Next, a *positive* in-plane field of 85 Oe was applied along the line of dots

from left to right in the in-plane MFM images. This procedure was continued for positive fields of up to 3010 Oe, as labeled in Fig. 11.

Note the evolution of the MFM images in Fig. 11. In the remanent state, the dots themselves show relatively little magnetic contrast, but the regions between dots (where there is perpendicular magnetic anisotropy) show a rich domain structure. This image shows a relatively uniform chainlike line of dots in the horizontal direction. This remanent state is quite different from that observed in the remanent state after saturation in a perpendicular field. As the in-plane field is increased, the rich domain structure observed in areas between dots diminishes in a regular fashion. By 3.01 kOe, there is very little magnetic contrast, and we conclude that the magnetization in the film is almost entirely pulled in plane, consistent with the observed in-plane hysteresis loops.

The domain structure seems quite complicated for both perpendicular field remanence and in-plane field remanence. This must be expected because the dot and background region moments are interacting with each other to minimize the overall energy. When a fairly modest field is applied in the perpendicular direction (Fig. 10, 183 Oe), the moments outside the dots will immediately align with the field since the coercivity of the unpatterned film is only 105 Oe. Thus, the perpendicular component (after patterning) will reverse direction quite easily as the field is increased. But the in-plane moments (in the dots) are much harder to pull out of plane, as is consistent with the perpendicular-to-plane hysteresis loops. As can be seen in Fig. 10, the contrast in the MFM image is substantially reduced at high applied perpendicular field.

As discussed before, one expects complicated interactions between the in-plane moments of the dots and the perpendicular moments that exist between the dots, and this can lead to complex domain structures. When the field is applied in plane, the moments that are pointing out of plane align with the field slowly because of the strong perpendicular anisotropy. This is the reason why we see more domain structure in the region between dots for field in plane, but not for field perpendicular. An interesting observation for in-plane fields is that the dots themselves are not as clearly defined as in the perpendicular field images. That is, one might expect the in-plane moments to be all aligned at fairly small field, which would lead to a distinctive MFM signature associated with north-south poles of adjacent dots along the field direction. No such signature is observed, suggesting that the moments in the regions to the left and right of each dot are quite strongly coupled to the moments in the dots, so that the signature is significantly reduced or absent.

IV. SUMMARY AND CONCLUSIONS

We have first used standard classical optical interference calculations to predict the light intensity distributions for two, three, and four interfering beams of light by developing a program using the algebraic computer program MAPLE to simulate the interference effects which occur when more than two beams interfere on the sample surface. We found that the predicted patterns could be controlled by varying the angles of incidence, the polarizations of the beams, and the wavelength and intensity of the beams. A wide variety of patterns was produced, and it was demonstrated that direct laser interference patterning (DLIP) technique can be effectively used to locally modify both the film topography and the material properties. It is also worthwhile to carry further such calculations under a wider variety of interfering beam geometries to see what additional complex periodic arrays might be formed, and this will be a subject of future investigations.

Finally, the DLIP technique developed by Polushkin and co-workers was used and extended to topographically and structurally modify several magnetic thin films and multilayers. In this technique, a pulsed Nd:YAG laser was utilized to split laser beam into two or three beams, which were then recombined on magnetic film surface. Interference between these beams results in intensity maxima which can locally modify both the film topography and the material properties, forming arrays of lines or dots. We have found that for smaller pulse energies the local laser heating on $[\mathrm{Co/Pt}]:\mathrm{SiO}_x$ films caused changes in the magnetic properties. AFM/MFM measurements showed that the magnetic properties were modified by the intense light, but not the film topography. X-ray diffraction measurements showed that structural changes brought about by patterning were quite modest. Magnet force microscopy and magneto-optic Kerr effect measurements showed considerable change after the DLIP process. In perpendicular hysteresis loops, the squareness was lost and the remanent magnetization M_r was decreased while the coercivity was increased. On the other hand, in the in-plane hysteresis loops, there was an increased squareness and an increase in the M_r value while the coercivity decreased. By comparing the shape and the changes in M_r before and after patterning, we concluded that the patterning process caused a transfer of perpendicular magnetization into an in-plane magnetization in the locally annealed regions, creating an "anisotropy" lattice on a region typically 3–4 mm in lateral dimensions with only one pulse of the laser. This shows a great promise of modification of material properties by DLIP.

We will continue to work on the magnetic properties of other systems, including a-$[\mathrm{Dy/Co}]:\mathrm{SiO}_2$ multilayers which show some similarities with $[\mathrm{Co/Pt}]:\mathrm{SiO}_x$ multilayers. There are many other magnetic systems that might yield quite interesting magnetic results such as locally induced magnetic or optical anisotropy induced in cobalt iron cyanide by laser beam irradiation.[41,42] DLIP may also be useful to modify various semiconductor systems. It may be possible, for example, to use local annealing with DLIP to laterally modulate doping levels in semiconductor heterostructures, with subsequent controllable changes in transport and optical properties.

ACKNOWLEDGMENTS

This research was supported by NSF-MRSEC, by the Center for Materials Research and Analysis, and by the Nebraska Research Initiative. We would like to thank Steve

Ducharme for loan of experimental apparatus and for a number of helpful discussions, and Yi Liu for electron microscopy measurements.

[1]S. Y. Chou, M. S. Wei, P. R. Krauss, and P. B. Fischer, J. Appl. Phys. **76**, 6673 (1994).
[2]V. White, R. Ghodssi, C. Herdey, D. D. Denton, and L. McCaughan, Appl. Phys. Lett. **66**, 2072 (1995).
[3]H. Tan, A. Gilbertson, and S. Y. Chou, J. Vac. Sci. Technol. B **16**, 3926 (1998).
[4]J. Shen, M. Klaua, P. Ohresser, H. Jenniches, J. Barthel, Ch. V. Mohan, and J. Kirschner, Phys. Rev. B **56**, 11134 (1997).
[5]V. Ng, Y. V. Lee, B. T. Chen, and A. O. Adeyeye, Nanotechnology **13**, 554 (2002).
[6]T. Scheibel, R. Parthasarathy, G. Sawicki, X. M. Lin, H. Jaeger, and S. L. Lindquist, Biophysics (Engl. Transl.) **100**, 4527 (2003).
[7]J. C. Huie, Smart Mater. Struct. **12**, 264 (2003).
[8]B. Kippelen, Nat. Mater. **3**, 841 (2004).
[9]P. Gambardella, S. Rusponi, T. Cren, N. Weiss, and H. Brune, C. R. Phys. (to be published).
[10]G. Carter, J. Phys. D **34**, R1 (2001).
[11]J. Lohau, A. Moser, C. T. Rettner, M. E. Best, and B. D. Terris, Appl. Phys. Lett. **78**, 990 (2001).
[12]G. Xiong, D. A. Allwood, M. D. Cooke, and R. P. Cowburn, Appl. Phys. Lett. **79**, 3461 (2001).
[13]M. Albrecht, C. T. Rettner, M. E. Best, and B. D. Terris, Appl. Phys. Lett. **83**, 4363 (2003).
[14]J. Li and C. Rau, Nucl. Instrum. Methods Phys. Res. B (to be published).
[15]A. Mougin *et al.*, J. Appl. Phys. **89**, 6606 (2001).
[16]A. Ehresmann, I. Krug, A. Kronenberger, and A. Ehlers, J. Magn. Magn. Mater. **280**, 369 (2004).
[17]W. Jung, F. J. Castaño, C. A. Ross, R. Menon, A. Patel, E. E. Moon, and H. I. Smith, J. Vac. Sci. Technol. B **22**, 3335 (2004).
[18]Y. Roussigne, S. M. Cherif, and P. Moch, J. Phys.: Condens. Matter **16**, 4591 (2004).
[19]K. Machidaa, T. Tezukab, T. Yamamotob, T. Ishibashib, Y. Morishitab, A. Koukitub, and K. Satob, J. Magn. Magn. Mater. (to be published).
[20]S. H. Liou, R. F. Sabiryanov, S. S. Jaswal, J. C. Wu, and Y. D. Yao, J. Magn. Magn. Mater. **226–230**, 1270 (2001).
[21]G. Hu *et al.*, J. Appl. Phys. **95**, 7013 (2004).
[22]J. I. Martin, J. Nogues, K. Liu, J. L. Vicent, and I. K. Schuller, J. Magn. Magn. Mater. **256**, 449 (2003).
[23]N. I. Polushkin, S. A. Gusev, M. N. Drozdov, Yu. K. Verevkin, and V. N. Petryakov, J. Appl. Phys. **81**, 5478 (1997).
[24]Yu. K. Verevkin, V. N. Petryakov, and N. I. Polushkin, Tech. Phys. Lett. **24**, 460 (1998).
[25]A. M. Alekseev, Yu. K. Verevkin, N. V. Vostokov, V. N. Petryakov, N. I. Polushkin, A. F. Popkov, and N. N. Salashchenko, JETP Lett. **73**, 192 (2001).
[26]M. Zheng *et al.*, IEEE Trans. Magn. **37**, 2070 (2001).
[27]M. Zheng *et al.*, Appl. Phys. Lett. **79**, 2606 (2001).
[28]L. Gao, S. H. Liou, M. Zheng, R. Skomski, M. L. Yan, D. J. Sellmyer, and N. I. Polushkin, J. Appl. Phys. **91**, 7311 (2002).
[29]N. I. Polushkin, J. Wittborn, C. Canalias, K. V. Rao, A. M. Alexeev, and A. F. Popkov, J. Appl. Phys. **92**, 2779 (2002).
[30]N. I. Polushkin, K. V. Rao, J. Wittborn, A. M. Alexeev, and A. F. Popkov, J. Magn. Magn. Mater. **258–259**, 29 (2003).
[31]Z. G. Li and P. F. Garcia, J. Appl. Phys. **71**, 842 (1992).
[32]Y. P. Lee, R. Gontarz, and Y. V. Kudryavtsev, Phys. Rev. B **63**, 144402 (2001).
[33]T. Suzuki, H. Notarys, D. C. Dobbertin, C.-J. Lin, D. Weller, D. C. Miller, and G. Gorman, IEEE Trans. Magn. **28**, 2754 (1992).
[34]T. K. Hatwar and C. F. Brucker, IEEE Trans. Magn. **31**, 3256 (1995).
[35]J. X. Shen, R. D. Kirby, K. Wierman, D. J. Sellmyer, and T. Suzuki, J. Appl. Phys. **73**, 6418 (1993).
[36]J. Ferré *et al.*, J. Magn. Magn. Mater. **198–199**, 191 (1999).
[37]C. Chappert *et al.*, Science **280**, 1919 (1998).
[38]T. Devolder, J. Ferré, C. Chappert, H. Bernas, J. P. Jamet, and V. Mathet, Phys. Rev. B **64**, 064415 (2001).
[39]B. D. Terris, L. Folks, D. Weller, J. E. E. Baglin, A. J. Kellock, H. Rothuizen, and P. Vettiger, Appl. Phys. Lett. **75**, 403 (1999).
[40]B. D. Terris, D. Weller, L. Folks, J. E. E. Baglin, A. J. Kellock, H. Rothuizen, and P. Vettiger, J. Appl. Phys. **87**, 7004 (2000).
[41]O. Sato, T. Iyoda, A. Fujishima, and K. Hashimoto, Science **272**, 704 (1996).
[42]G. L. Gutsev, B. V. Reddy, S. N. Khanna, B. K. Rao, and P. Jena, Phys. Rev. B **58**, 14131 (1998).